T. SADOWSKI*, M. KNEĆ*

APPLICATION OF DIC TECHNIQUE FOR MONITORING OF DEFORMATION PROCESS OF SPR HYBRID JOINTS

ZASTOSOWANIE TECHNIKI DIC DO OBSERWACJI PROCESU DEFORMACJI HYBRYDOWYCH POŁĄCZEŃ TYPU SPR

Digital Image Correlation (DIC) technique gives possibility to observe deformation process in many applications including self-piercing riveting (SPR) hybrid joint. The hybrid SPR joint consists of simple SPR joint made of two adherends, steel tubular rivet (total length of 5 mm) and an adhesive. The adhesive was applied before piercing process.

For specimen preparation two different aluminum alloys were used: 2024 and 5005 (2mm thickness both) with tensile strength 400 and 160MPa, respectively. For better understanding of joint forming process and to allow DIC strains observation during the joint creation, a special holder was designed with precisely polished die. The tests were performed by application of the 100kN servo-hydraulic machine, which recorded time, load, displacement and was synchronized with the DIC system.

The joint forming process was carried out with 2 mm/min constant speed. During piercing process rivet and upper surface of the adherend were observed and the major strain states were estimated. The uniaxial tensile tests of single lap joints (SLJ) up to the final failure were performed and the displacements and the strains were recorded. In particular the rivet deformation was observed also during the whole loading process.

The hybrid SPR joints are very effective, because the load capacity and energy absorption increase more than 1.5 times in comparison to the simple SPR joints.

Keywords: DIC, SPR, joining process, hybrid joint

Technika Cyfrowej Korelacji obrazu (DIC) pozwala na obserwacje procesów deformacji w różnych aplikacjach – w tym dla hybrydowych połączeń typu SPR (przebijanych za pomocą nita). Hybrydowe połączenie typu SPR składa się ze standardowego połączenia SPR – próbka jednozakładowa przebita stalowym nitem pół-rurkowym (długość całkowita 5 mm) oraz warstwy kleju pomiędzy zakładkami naniesionego przed procesem przebijania.

Do stworzenia próbek zostały użyte dwa typu aluminium o różnej plastyczności 2024 i 5005 o grubości 2 mm każdy i wytrzymałości odpowiednio 400MPa i 160 MPa. W celu pełniejszego zrozumienia procesu formowania się złącza został zaprojektowany specjalny uchwyt z precyzyjnie wyszlifowaną matrycą. Badania zostały przeprowadzone przy pomocy maszyny osiowej o zakresie 100kN, zsynchronizowaną z systemem DIC.

Proces tworzenia się złącza był prowadzony ze stałą prędkością 2 mm/min. Podczas procesu tworzenia złącza obserwowano nit oraz górną powierzchnię łączonych blach i główne odkształcenia zostały wyznaczone. Badania przeprowadzono na próbkach zakładkowych do ich zniszczenia rejestrując przemieszczenia i odkształcenia. W szczególności obserwowano deformację nita w całym procesie deformacji.

Hybrydowe połączenia typu SPR są bardzo efektywne, ponieważ uzyskuje się wzrost siły przenoszonej przez połączenie i energii absorbowanej ponad 1.5 raza większych w porównaniu do prostego złącza typu SPR.

1. Introduction

The current challenges in designing of modern aircrafts as for weight reduction, fuel consumption reduction, increasing of security, reliability and reduction of maintenance costs lead to seeking for new technological solutions in the field of:
- discovering of innovative materials
- creation of original solutions for joining Principal Structural Elements (PSE) of airplanes made of new composite materials (for example the fuselage airframe section is a PSE).

The innovative materials are usually bulid up from different phases, properly selected in order to get better theromechanical properties, which are able to satisfy extremal working conditions of different elements of the aircrafts (e.g. engines, wings, fuselage, etc.). During modern technological process it is possible to create controlled internal structure of the multiphase materials, which can satisfy designers' demands and operation conditions of the airplane. In terms of strength, heat resistance, or some other desired characteristic, the composite must reveal better properties than each component alone. One can distinguish particle reinforced composite materials (e.g. [1-4]), composites with intergranular plastic layers (e.g.

* LUBLIN UNIVERSITY OF TECHNOLOGY, 20-618 LUBLIN, 40 NADBYSTRZYCKA STR., POLAND

[5-8]) or so called "functionally graded materials" (FGM), e.g. [9-14]. A certain amount of porosity is necessary to satisfy designers' requirements for specific applications, e.g. [15-18].

Even in the case of joining PSE parts instead of using classical adhesives (e.g. [19-26]) one can observe the application of new types of adhesives, which contain nanoparticles (e.g., carbon nanotubes [27], SiO_2 nanoparticles [28] or graphene) to modify specific properties (e.g. electric conductivity [27, 28]). This adhesive layer can be treated as a particle reinforced composite.

Other relatively new ideas in the joining of structural parts (e.g. the PSE) are so called hybrid joints, which result from combination of two single joining techniques, e.g. [19-25] and [28-30]. In this paper we focus on the technology and experimentation of the adhesive aided self-piercing riveting (SPR) joint of the PSE. Some aspects of designing process of simple SPR was described in [30].

Experiments were done for hybrid single lap joints (SLJ) with application of the SPR and adhesive bonding. Digital Image Correlation (DIC) technique gives possibility to observe the whole deformation process, starting from the forming of the SPR and further monitoring of different stages of the SLJ mechanical response up to the final failure.

Combination of the two mentioned techniques significantly improves the overall mechanical response of the joint. As a result of the investigations one can observe significant increase of the strength and increase of the energy absorption (EA) almost 2 times. This leads to increase of fatigue properties.

2. Technology of the adhesive aided SPR joints

In order to create the adhesive aided SPR joint it is necessary to have a properly shaped die and a system to hold joined materials. The harder material for production of a tubular rivet is required also. The technological idea of the SPR joint is presented in Fig. 1. It obeys: 1 – positioning of the system, 2 – initial perforation of the top sheet, 3 – forming of the SPR and 4 – unloading.
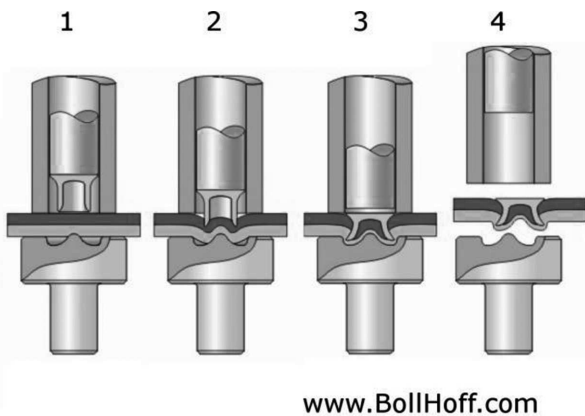

Fig. 1. Technology of the SPR joint creation: 1 – positioning, 2 – initial perforation, 3 – forming, 4 – unloading of the system

For our investigations two types of dies has been prepared taking into account the geometry described in [30] and [31]. The hybrid joints consisted of: two aluminum stripes – 2024

T4, and 5005, the steel tubular rivet acquired from Bollhoff Company and Loctite 3423 adhesive.
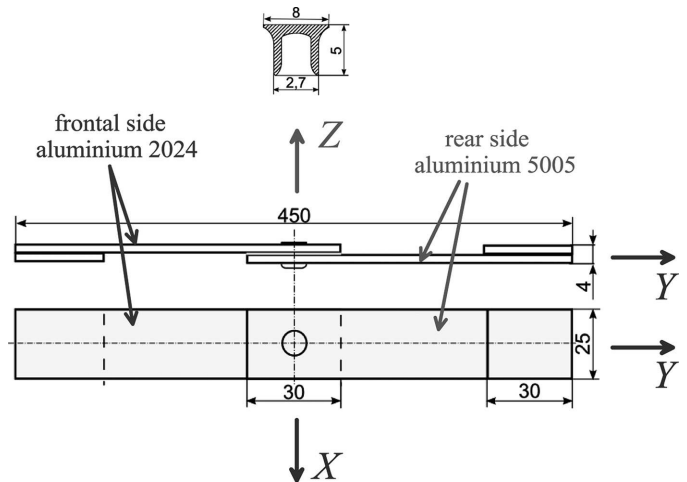

Fig. 2. Rivet C-SKR by Bollhoff, and the hybrid SPR specimen dimensions

In order to compare effectiveness of the hybrid joints with additional layer of the adhesive a set of samples with the SPR mechanical connection only was prepared. Dimensions of the specimen and shape of the rivet are shown on the Fig. 2. Information containing basic data for joined components are presented in Table 1.

TABLE 1

Strength of the materials used for SPR-bonded joints

Material	Characteristic strength
Aluminum 2024 T4	$R_m = 400$ MPa
Aluminum 5005	$R_m = 160$ MPa
Boron steel (rivet)	$R_m = 950$ MPa
Loctite 3423	$\tau_{max} = 10$ MPa

Technological data concerning manner of specimens preparation are presented in the Table 2. One can point out that we analysed two speeds of piercing process – standard – 2mm/min and a very quick 200 mm/min.

TABLE 2

Technological data for specimens preparation

Technological operations	Data
Clamping torque for each of four M6 screws	8 Nm
Speed of piercing for standard joint	2 mm/min
Speed of piercing for non standard joint	200 mm/min
Adhesive thickness (measured before test)	$5 \mu m$
Curing time	30 minutes
Curing temperature	$80°C$

3. Experimental technique for testing of hybrid joints

The experimental stand is presented in Fig. 3. It consists of: MTS 100 kN servohydraulic testing machine, Aramis DIC system. In order to form the SPR joint we used a die, a punch and 2 very stiff blankholders. The blankholders (2) keep stable the aluminum stripes of the SLJ (4) in place during piercing by punch (7). Then the piercing process starts with 2 different velocities. The whole forming process was monitored with the DIC system, which allows for observations of all stages of deformation. The SLJ specimens were made of two different aluminum strips, Fig. 2. The upper one was made of the aluminum alloy 2024 – stiffer material (Table 1) with smaller plasticity, whereas the lower strip was prepared from aluminum alloy 5005, which exhibits higher formablity during piercing. In this case we got properly created bottom side of the SPR joint, Fig. 4a. Changing of the strip sequence leads to cracks initiation in less plastically deformed strip made of aluminum alloy 2024 (Fig. 4 b).
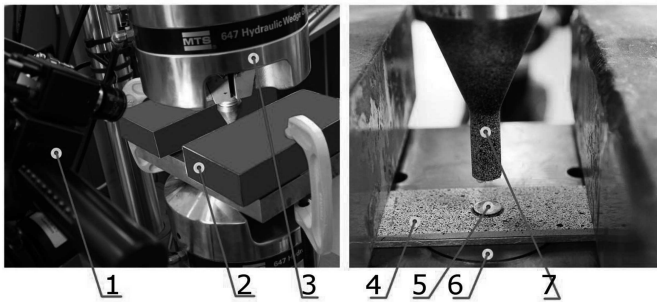

Fig. 3. DIC testing stand for piercing monitoring, 1 – DIC sensor, 2 – blankholders, 3 – MTS servohydraulic machine, 4 – top aluminum 2024 strip, 5 – C-SKR rivet, 6 – die, 7 – punch

Distance between the blankholders results from the DIC sensor cameras (1), i.e. angle and distance was kept as small as possible to see the punch (7), the rivet (5) and the aluminum stripes (4) placed in the central position of the die (6) axis. Before the piercing process the rivet (5) was always centered above the die, then it was lifted up by punch (7), and finally die (6) was fixed to start in the next stage forming process of the SPR. This procedure allows to have repeatable piercing joints.
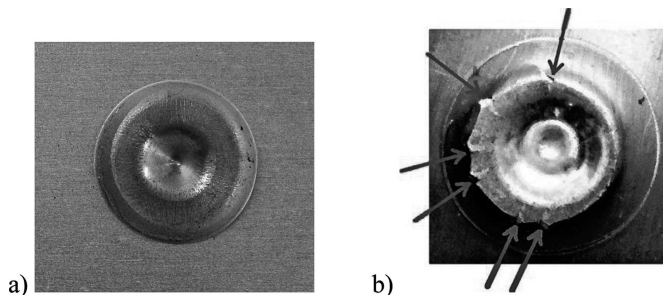

Fig. 4. Rear specimen side view: a) properly created joint (aluminum 5005), b) cracks on (aluminum 2024)

Contour view overlapped on the polished cross sections (Fig. 5a) shows the proper hybrid joint having the die geometry proposed in [30] with 1mm cone offset and the piercing length of 5,5 mm. Fig. 5b shows the joint prepared in not corrected way - having the die shape according to [31], i.e. without the cone offset with the rivet pierced for 5mm. The piercing length equals to 5,5 mm results from difference between not deformed rivet and the average value taken from measurements of the five rivet lengths after forming process.
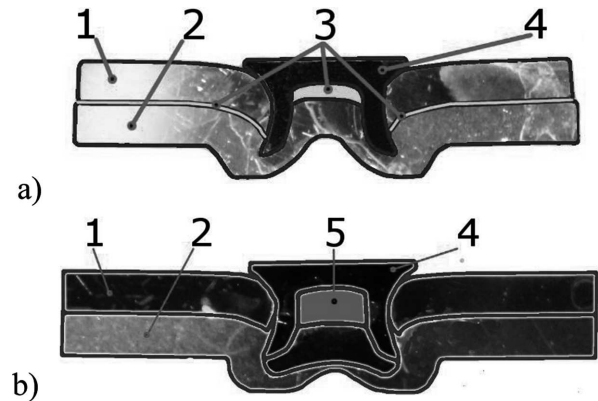

Fig. 5. a) correctly formed the hybrid SPR joint obtained with the die having the cone offset [31], b) incorrect the SPR joint, where 1 – aluminum alloy 2024, 2 – aluminum alloy 5005, 3 – loctite 3423 adhesive, 4 – steel rivet C-SKR by Bollhoff, 5 – empty space

In case of application of the die without cone offset [31] (Fig. 5b) we get empty area under the rivet head, not filled by the adherends material. This causes decrease of overall stiffness of the joint, friction between the rivet and the joining materials and finally leads to significantly lower load capacity of the joint.

Leveling the rivet head with the top adherend surface by using the die with the offset results in increase of stiffness and the load capacity. The adhesive was applied before positioning the material strips in the base. Adhesive flushes were removed from the joint before heating. The adhesive applied inside the rivet before piercing additionally fills free volume and creates adhesion forces in the joint between the rivet and aluminum 2024, cut firstly at the beginning of piercing.

This procedure was chosen as the optimal for all hybrid SPR joints. Just after manufacturing each specimen was heated up to 80°C for 30 minutes for curing, and then they were tested after at least 24 hours.

4. Results and discussion

Typical load – displacement curves for piercing process for the simple SRP and the hybrid joints are presented in Fig. 6.

Piercing procedure is determined by several characteristic points. In the first stage up to the point I (Fig. 6a) we have an elastic part of the joining process. Maximum of the load before piercing of the hole in aluminum 2024 (the top strip) is denoted by – II. Then load drops until point III, and we have almost flat part of the diagram after cancelling looses in the joint (point IV). Then load increases up to point V, where the maximum displacement of the rivet is reached.

The load – displacement curves in Fig. 6a and 6b are similar, but the obtained plots for the hybrid SPR forming with the die having the offset are more scattered. The average maximal load in Fig. 6a (5mm depth) is 36,3 kN, whereas for

rivet leveling with the top aluminium strip (5,5 mm piercing depth) average load is 44,3 kN, i.e. the load increase corresponding to 0.5mm displacement of the rivet increase is equal to 22%.
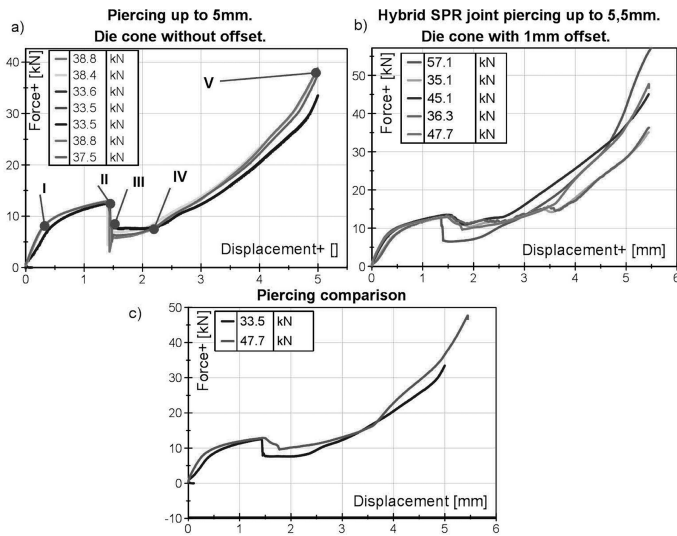

Fig. 6. Load-displacement diagram for piercing process:
a) piercing up to 5 mm using the die without the cone offset,
b) piercing up to 5,5 mm using the die with the 1mm cone offset,
c) comparison between piercing with the use of the die with the cone offset and without this offset.
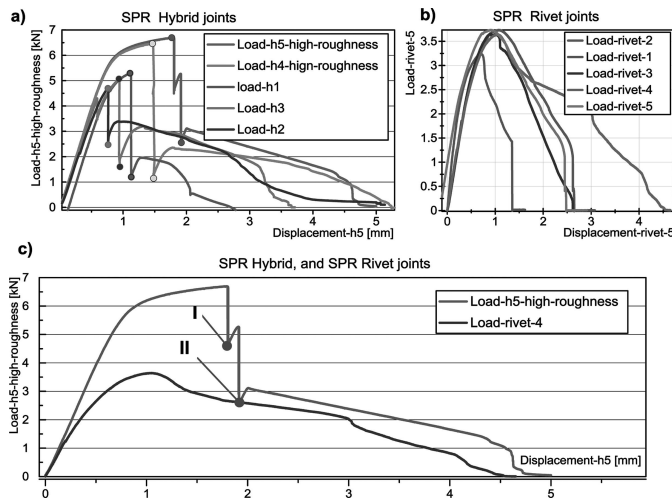

Fig. 7. Load – displacement tensile tests: a) the hybrid SPR joints, b) the pure SPR joint, c) comparison of the hybrid and pure SPR joints

The load – displacement correlations after tensile tests with 2mm/min speed are presented in Fig. 7. Fig. 7b presents experimental curve for the simple SPR joints. One can notice a very good tests repeatability. It also indicates that the elaborated technology of the SPR and the hybrid joints manufacturing was very good.

The experimental load-displacement curves for hybrid joints (Fig. 7a) show the results for two different types of specimens, reveal different roughness of the bonding adherends in the overlapping region. One of them was prepared with application only of the abrasive paper of type 120 – the specimen h1-h3. The second specimens (h4 and h5) with the paper 120

and several deep cuts made manually using sharp cutter in the adjacent sides of the joined aluminum strips (Fig. 8). The objective for increasing roughness is to keep the adhesive inside
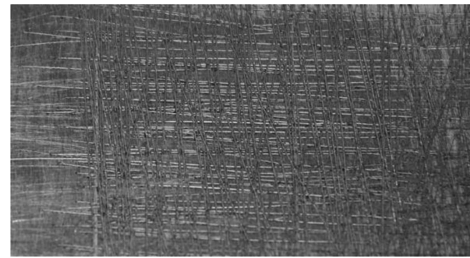

Fig. 8. Perpendicular cuts increasing roughness

grooves during fixing and piercing. The specimens h4 and h5 (Fig. 7a) with higher roughness of the joining surfaces exhibit significantly higher load capacity in comparison to the simple SPR joint equal to 76%. The roughness created only by abrasive paper was not enough to keep higher volume content of the adhesive between the material stripes, which flows out during piercing and fixing process. In these specimens (h1 – h3) the corresponding increase of the load capacity is approximately 30% higher in comparison to the simple SPR joint.

In the SLJ specimen under uniaxial tension the overlapping region is subjected to bending due to an off-center loading. It creates very complex 3-D state of deformation, which can be monitored only with application of the DIC. The displacement U_z (Fig. 9a) presents behavior of the specimen in Z direction measured in four points in the rear specimen side (Fig. 3b). Point 0 and 1 were selected from the die area and points 2 and 3 were chosen in the surrounding region, but very close to the SPR. The shapes of these functions are similar, but they differ in values.

The rivet head (front specimen side) behaves symmetrically in relation to the rear specimen side. All the displacements are measured in relation to the reference stage – number 0 (Fig. 9).

Diagrams in Fig. 9d – h present the displacement U_z of the longitudinal cross section of the joint (along the coordinate Y) along the length of the specimen across the sections made of aluminum 2024 and aluminum 5005. In the first two plots (Fig. 9d,e) the longitudinal cross section is continuous line which means that the joint is working as one element. At the maximum load debonding process starts (Fig. 9e) from the front part of the joint. There is still contact between both adhereds and half of the joint is still carrying the uniaxial load (Fig. 9f). Fig. 9g presents debonding initiation from the rear part of the joint. With the increase of deformation process we observe total debonding and only the SPR curries the load. Finally, Fig. 9h presents failure of the hybrid joint.

During piercing the upper material (2024) deforms with the finite strains because of penetration of the adherends by the rivet. The size of this finite strain zone can be observed by DIC technique and moreover we recorded major strain during piercing process, Fig. 10. The DIC system allows for creation of maps of the major strains for different stage of the load – displacement curve. Vertical axis presents the major strain distribution around the rivet head. It can be clearly seen that the shape of the deformation zone does not change significantly after the first maximum of the load, before piercing of the first

aluminum strip 2024. The corresponding views of these maps on the *XY* plane are presented in Fig. 11, where the highly deformed regions are presented by white circles.
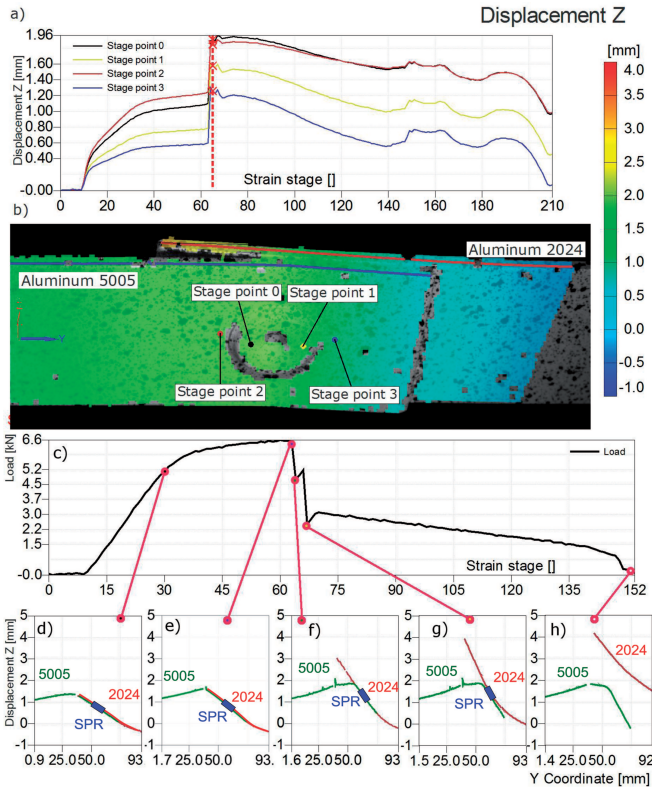

Fig. 9. Displacements U_z estimated using the DIC system: a) the displacement U_z in four selected points, b) localization of the stage points (1 to 4) in the strips made of aluminum 2024 (green colour) and aluminum 5005 (red colour), c) the load – displacement curve, d) the displacement U_z of the longitudinal cross section of the joint in the yield point, e) the displacement U_z of the longitudinal cross section of the joint in maximum load, f) the displacement U_z of the longitudinal cross section of the joint in debonding initiation, g) the displacement U_z of the longitudinal cross section of the joint in final debonding, h) the displacement U_z of the longitudinal cross section of the joint in the final failure moment

Fig. 10. Deformation zone in 3D analysis of particular points using the major strain of the DIC technique

The deformed zone diameter obtained with the DIC measurement is equal to 15 mm (Fig. 11) for specimen dimensions presented on Fig. 2. Condition for calculation of this diameter was that the threshold value of the major strains ε_{major} >0,4%. This value 0.4% o results from noise analysis made by the DIC system on two first stages without load.
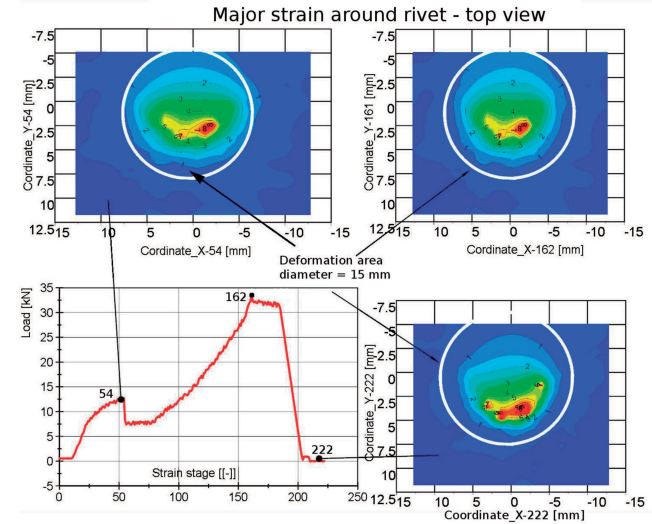

Fig. 11. Deformation zone near the SPR – top view

5. Conclusions

DIC technique allows for observation of the 3-D displacements distribution near the rivet through the whole deformation process. Proper setting of the system permits to record two perpendicular surfaces during tensile tests of the SPR joint. The results presented in Fig. 9 show when hybrid joint is carrying the load. Investigation of deformation zone (Fig. 10 and 11) are not possible without DIC technique.

Creation of the hybrid joint made of the SPR and adhesive bonding significantly improves the overall mechanical response of the joint. As a result of the investigations one can observe significant increase of the strength (about 76%) and increase of the energy absorption (EA) almost 2 times. This leads to increase of fatigue properties of the joints.

This investigation will be developed further to create the numerical model of the joint, which will take into account gradual degradation of the adhesive layer and cracking process in the plastic adherends, in order to extend previously formulated damage and cracking models for materials (e.g. [32-39] and other types of the hybrid joints [19-25] and [28-30]).

Acknowledgements

124

REFERENCES

[1] S. N e m a t - N a s s e r, M. H o r i, Micromechanics: overall properties of heterogeneous materials, Elsevier, 2nd ed., ISBN 0-444-50084-7, Holland (1999).

[2] M.J. P i n d e r a, H. K h a t a m, A.S. D r a g o, Y. B a n s a l, Micromechanics of spatially uniform heterogeneous media: A critical review and emerging approaches, Comp. Part B **40**, 349-378 (2009).

[3] M.A.A. C a v a l c a n t e, M.J. P i n d e r a, H. K h a t a m, Finite-volume micromechanics of periodic matrials: Past, present and future, Comp. Part B **43**, 2521-2543 (2012).

[4] S. S c h m a u d e r, L. M i s h n a y e v s k y Jr., Micromechanical and Nanosimulation of Metals and Composites, Springer-Verlag, Berlin Heidelberg, 2009.

[5] T. S a d o w s k i, S. H a r d y, E. P o s t e k, Prediction of the mechanical response of polycrystalline ceramics containing metallic inter-granular layers under uniaxial tension. Comput. Mat. Sci. **34**, 46-63 (2005).

[6] T. S a d o w s k i, S. H a r d y, E. P o s t e k, A new model for the time-dependent behaviour of polycrystalline ceramic materials with metallic inter-granular layers under tension. Mat. Sci. Eng. A **424**, 230-238 (2006).

[7] T. S a d o w s k i, E. P o s t e k, Ch. D e n i s, Stress distribution due to discontinuities in polycrystalline ceramics containing metallic inter-granular layers. Comput. Mat. Sci. **39**, 230-236 (2007).

[8] T. S a d o w s k i, T. N o w i c k i, Numerical investigation of local mechanical properties of WC/Co composite, Comput. Mat. Sci. **43**, 235-241 (2008).

[9] S. S u r e s h, A. M o r t e n s e n, Fundamentals of Functionally Graded Materials, Institute of Materials, London, 1998.

[10] T. S a d o w s k i, M. B o n i e c k i, Z. L i b r a n t, K. N a k o n i e c z n y, Theoretical prediction and experimental verification of temperature distribution in FGM cylindrical plates subjected to thermal shock. Int. J. Heat and Mass Transfer **50**, 4461-4467 (2007).

[11] T. S a d o w s k i, S. A t a y a, K. N a k o n i e c z n y, Thermal analysis of layered FGM cylindrical plates subjected to sudden cooling process at one side – comparison of two applied methods for problem solution, Comp. Mater. Sci. **45**, 624-632 (2009).

[12] T. S a d o w s k i, A. N e u b r a n d, Estimation of the crack length after thermal shock in FGM strip, Int. J. Fract. **127**, 135-140 (2004).

[13] K. N a k o n i e c z n y, T. S a d o w s k i, Modelling of thermal shock in composite material using a meshfree FEM, Comp. Mater. Sci. **44**, 1307-1311 (2009).

[14] T. S a d o w s k i, K. N a k o n i e c z n y, Thermal shock response of FGM cylindrical plates with various grading patterns, Comput. Mat. Sci. **43**, 171-178 (2008).

[15] T. S a d o w s k i, S. S a m b o r s k i, Prediction of mechanical behaviour of porous ceramics using mesomechanical modelling. Comput. Mat. Sci. **28**, 512-517 (2003).

[16] T. S a d o w s k i, S. S a m b o r s k i, Modelling of porous ceramics response to compressive loading. J. Am. Cer. Soc. **86**, 2218-2221 (2003).

[17] T. S a d o w s k i, S. S a m b o r s k i, Development of damage state in porous ceramics under compression. Comput. Mat. Sci. **43**, 75-81 (2008).

[18] E. P o s t e k, T. S a d o w s k i, Assessing the Influence of Porosity in the Deformation of Metal-Ceramic Composites, Composite Interfaces **18**, 57-76 (2011).

[19] T. S a d o w s k i, M. K n e ć, P. G o l e w s k i, Experimental investigations and numerical modelling of steel strip adhesive joint reinforced by rivets, Int. J. Adhes. & Adhes. **30**, 338-346 (2010).

[20] T. S a d o w s k i, P. G o l e w s k i, E. Z a r z e - k a - R a c z k o w s k a, Damage and failure processes of hybrid joints: Adhesive bonded aluminium plates reinforced by rivets, Comput. Mat. Sci. **50**, 1256-1262 (2011).

[21] T. S a d o w s k i, T. B a l a w e n d e r, Technology of Clinch – Adhesive Joints, in Hybrid adhesive joints. Advanced Structured Materials, Volume 6, Springer 2011, L. F. M. da Silva, A. Pirondi, A. Öschner (Eds), pp. 149-176.

[22] T. B a l a w e n d e r, T. S a d o w s k i, P. G o l e w s k i, Experimental and numerical analyses of clinched and adhesively bonded hybrid joints, J. Adhes. Sci Technol. **25**, 2391-2407 (2011).

[23] T. B a l a w e n d e r, T. S a d o w s k i, M. K n e ć, Technological problems and experimental investigation of hybrid: clinched – adhesively bonded joint, Arch. Metall. Mat. **56**, 439-446 (2011).

[24] T. B a l a w e n d e r, T. S a d o w s k i, P. G o l e w s k i, Numerical analysis and experiments of the clinch-bonded joint subjected to uniaxial tension, Comput. Mat. Sci. **64**, 270-272 (2012).

[25] T. S a d o w s k i, T. B a l a w e n d e r, Technology of Clinch – Adhesive Joints, in Hybrid adhesive joints. Advanced Structured Materials, Volume 6, Springer 2011, L. F. M. da Silva, A. Pirondi, A. Öschner (Eds), pp. 149-176.

[26] Z. W u, J. L i, D. T i m m e r, K. L o r e n z o, S. B o s e, Study of processing variables on the electrical resistivity of conductive adhesives, Int. J. Adhes. & Adhes. **29**, 488-494 (2009).

[27] H. Z h a o, T. L i a n g, B. L i u, Synthesis and properties of copper conductive adhesives modified by SiO_2 nanoparticles, Int. J. Adhes. & Adhes. **27**, 429-433 (2007).

[28] L.F.M. d a S i l v a, A. Ö c h s n e r, A. P i r o n d i (Eds), Hybrid adhesive joints, Springer (2011).

[29] F. M o r o n i, A. P i r o n d i, F. K l e i n e r, Experimental analysis and comparison of the strength of simple and hybrid structural joints, J. Adh&Adhes **30**, 367-379 (2010).

[30] G. D i F r a n c o, L. F r a t i n i, A. P a s t a, Analysis of the mechanical performance of hybrid (SPR/bonded) single-lap joints between CFRP panels and aluminum blanks, Int. J. Adh.&Adhes. (2012) DOI: http://dx.doi.org/10.1016/j.ijadhadh.2012.10.008367-379.

[31] J. M u c h a, Some aspects of designing process self piercing riveting. Archives of Mechanical Technology and Automation **29**, 4, 91-101 (2009).

[32] V. B u r l a y e n k o, T. S a d o w s k i, Influence of skin/core debonding on free vibration behaviour of foam and honeycomb cored sandwich plates, Int. J. Non-Linear Mechanics **45**, 959-968 (2010).

[33] V. B u r l a y e n k o, T. S a d o w s k i, Analysis of structural performance of aluminium sandwich plates with foam-filled hexagonal foam, Comp. Mater. Sci. **45**, 658-662 (2009).

[34] V. B u r l a y e n k o, T. S a d o w s k i, Effective elastic properties of foam-filled honeycomb cores of sandwich panels, Comp. Structures **92**, 2890-2900 (2010).

[35] L. M a r s a v i n a, T. S a d o w s k i, Stress intensity factors for an interface kinked crack in a bi-material plate loaded normal to the interface. Int. J. Fract. **145**, 237-243 (2007).

[36] L. M a r s a v i n a, T. S a d o w s k i, Fracture parameters at bi-material ceramic interfaces under bi-axial state of stress. Comp. Mater. Sci. **45**, 693-697 (2009).

[37] T. Sadowski, L. Marsavina, N. Peride, E.-M. Craciun, Cracks propagation and interaction in an orthotropic elastic material: analytical and numerical methods, Comput. Mat. Sci. **46**, 687-693 (2009).

[38] L. Marsavina, T. Sadowski, Kinked cracks at a bi-material ceramic interface – numerical determination of fracture parameters. Comput. Mat. Sci. **44**, 941-950 (2009).

[39] T. Sadowski, G. Golewski, Effect of aggregate kind and graining on modelling of plain concrete under compression, Comput. Mat. Sci. **43**, 119-126 (2008).